Final Draft
of the original manuscript:

Yang, J.; Lu, X.; Blawert, C.; Di, S.; Zheludkevich, M.L.:
Microstructure and corrosion behavior of Ca/P coatings prepared on magnesium by plasma electrolytic oxidation
In: Surface and Coatings Technology (2017) Elsevier

DOI: 10.1016/j.surfcoat.2017.04.001

Microstructure and Corrosion Behavior of Ca/P Coatings Prepared on Magnesium by Plasma Electrolytic Oxidation

Junjie Yang[a,b*], *Xiaopeng Lu*[b], *Carsten Blawert*[b], *Shichun Di*[a*], *Mikhail L. Zheludkevich*[b,c]

a) School of Mechatronics Engineering, Harbin Institute of Technology, West Dazhi Road 92, 150001 Harbin, P.R China

b) Institute of Materials Research, Helmholtz-Zentrum Geesthacht, Max-Plank-Str. 1, 21502 Geesthacht, Germany

c) Faculty of Engineering, University of Kiel, Kaiserstrasse 2, 24143 Kiel, Germany

Abstract

In order to enhance the corrosion resistance and biocompatibility of Mg based implants, porous MgO-CaP coatings were fabricated on commercial Mg by adding hydroxyapatite (HAp) particles in alkaline phosphate solution for plasma electrolytic oxidation (PEO) treatment. The effects of particle concentration on the coating morphology and composition were investigated under constant current PEO processing. Electrochemical impedance spectroscopy (EIS) and immersion test conducted in simulated body fluid (SBF) environment were applied to evaluate the corrosion performance of the coatings. The results showed that most HAp particles were reactively incorporated into the PEO coatings and the coating microstructure was significantly modified with increasing concentration of HA, which resulted in higher corrosion resistance in return. The consecutive growth of impedance during 72h immersion resulted from the precipitation and deposition of CaP compound and corrosion product into the pores sealing the defects of PEO coatings. Overall, a higher concentration (20g/L) of HAp particles addition would bring out a denser and protective PEO-HAp coating.

Key words: Magnesium; Plasma electrolytic oxidation; Hydroxyapatite; Corrosion

1 Introduction

It is well known that magnesium and its alloys are not only used in transport applications where weight reduction is of great importance, but can also be employed in manufacturing biodegradable implants for orthopedic and trauma surgery [1, 2]. Mg is an essential element and present in the human body, since it is directly related with many metabolic reactions and biological mechanisms [3, 4]. Also, the specific density and Young's modulus of Mg are close to those of human bone. And this feature decreases the stress shielding effects at the implant/bone interface, reducing the possibility of secondary injury. From the aspect of physiology, Mg-based alloys degrade gradually with the healing of tissue around the wound. This could prevent the secondary operation and the risk of infection. However, their rapid corrosion behavior in vivo environment is often seen as the critical factor that restricts the application of Mg alloys as biodegradable implants in clinical practice. The generation of a large volume of hydrogen gas and the significant increment of local pH value of body fluid can lead to the necrosis of tissues, blood stream blockage and even the patient's death [5]. Hence, controlling the corrosion and degradation rate in human body fluid environment is an imperative issue for promoting the application of Mg as implant material.

To solve these problems, many surface treatment methods have been studied and applied on Mg implants, such as chemical etching, electro-/electroless deposition, sol-gel coatings, chemical/physical vapor deposition and thermal spraying, etc [6-9]. Among these techniques, plasma electrolytic oxidation (PEO) is a powerful method for producing an oxide coating on the substrate, which significantly reduces the tendency of the metal to corrode and wear out. Three interdependent requirements determine the bone-forming ability of a bone substitute: scaffolding

for oesteoconduction (both mineral and collagen), growth factor for osteoinduction (noncollagenous bone matrix proteins) and progenitor cells for osteogenesis [10, 11]. Based on these aspects, Mg-PEO coatings can provide a controllable surface roughness and stable composition. However, unavoidable defects caused by the discharges (leading to pitting corrosion) [12] and poor bioactivity (retarding the adsorption and reproduction of osteoblast) [13] remain a concern.

Calcium phosphorus compounds, especially in form of hydroxyapatite (HAp), biphasic calcium phosphates and β-tricalcium phosphate, are advantageous and safe candidates for implants, since they are the main composition of human bones (37.5 wt.%: Ca 25.9%, P 11.6%) [14-16]. The abundance of calcium phosphate can activate not only bioactivity of implants, but also accelerate the healing process of wound in body fluid environment. Several approaches have been grafted with PEO technique for fabricating protective calcium phosphate coatings on implant surface. Electrolytes containing calcium phosphate salts (calcium glycerophosphate (CaGP), calcium citrate/acetate and sodium phosphate) were introduced by Gnedenkov and Tang [17-19]. It was found that the Ca/P ratio and microstructure of PEO coating was correlated with the amount of alkali and, under some circumstance (e.g. bipolar power regime), the PEO coatings required a further post-treatment to treat the defects left on the surface. Liu et al. deposited calcium deficient hydroxyapatite and dicalcium phosphate dehydrate (DCPD) on PEO coating by a chemical conversion method. They have reported the formation of hydroxyapatite on the coating surface during the incubation in SBF solution, and the decrease of released hydrogen volume [12, 20]. The synthesis of CaP substance by sol-gel method is suggested by Seyfoori et al.. With adding sol-gel HAp nano powder into electrolyte, nanostructured biphasic calcium phosphate (BCP) was detected. The further characterization showed that the enhanced corrosion resistance of

composite coating was related to the blocking feature of nanoparticles, and greater apatite forming ability was confirmed [15]. Gao et al. fabricated PEO-hydroxyapatite (HAp) coating by cathophoretic deposition. They claimed that corrosion resistance of Mg substrate was promoted by PEO coating and additional HA layer. After immersion test in physiological environment, Ca/P ratio increased for PEO coating but decreased for PEO-HAp coating [21]. Although quasi-calcium phosphate compounds are procurable through organizing the electrolyte composition or different multi-step post treatments, some concerns still remain there. The coating morphology and properties of PEO coating is greatly dependent on the electrolyte and power regime. Inappropriate composition and concentration of electrolyte would probably result in heterogeneous structure and/or introduce inevitable elements into the oxide coatings. Similarly, the complicated synthesis process and cohesion strength between the post-deposited HAp layer and PEO coating is rarely reported.

Incorporating foreign particles into PEO coatings is recognized as a promising and effective method for controlling the porosity or even introducing some functional properties to PEO coatings. The effects of particles addition on coating properties after incorporation are determined if particles are inert or reactively incorporated. A variety of particles (e.g. Al_2O_3, ZrO_2, TiO_2, CeO_2 and clay etc.) have been successfully incorporated into PEO coatings with enhancing the coating properties to some extent [22-27]. In present work, a simple approach is proposed to fabricate PEO-CaP composite coating on pure Mg substrate by in-situ suspending commercial HAp particles into the basic alkaline phosphate electrolyte. The influence of HAp concentration and processing parameters on coating growth dynamics, morphology as well as composition is studied with SEM, GIXRD and EDS, respectively. Besides, electrochemical impedance

spectroscopy (EIS) and immersion tests are applied for evaluating the corrosion performance in short-term and long-term degradation behavior of the coatings.

2 Experimental

2.1 Material

Rectangular specimens (25×25×4 mm) of commercial magnesium (hp-Mg) were used as substrates for PEO processing. The chemical composition measured by Spark OES (Spark analyser M9, Spectro Ametek, Germany) is 0.0129 wt.% Al, 0.00325 wt.% Ca, 0.00538 wt.% Fe, 0.0201 wt.% Mn, 0.00178 wt.% Zn, 0.0207 wt.% Si and Mg balance. The specimens were ground using emery papers up to 1200 grit, and degreased with ethanol prior to PEO treatment. Commercial HAp (CAS: 1306-06-5) was purchased from ACROS ORGANICS (USA), and it was used without any further purification. The SEM image of used HAp particles is given in Fig. 1. As shown, the HAp particles presented flake shape with particle size ranging from hundreds of nanometer to a few micrometers.

2.2 PEO treatment

As-received specimen and stainless steel tube were used as the anode and cathode respectively during PEO treatment. Basic alkaline solutions containing KOH (2g/L) and Na_3PO_4 (10g/L) with different concentrations of dispersed HAp particle (5, 10 and 20g/L) was used as coating electrolytes. All chemicals are reagent grade and used as received. All PEO treatments were performed for 10 min with fixed duty cycle (ratio between duration of the voltage pulse and total time of each cycle) of 20% and frequency of 200Hz provided by a DC pulse power source. All the treatments were conducted in constant current mode with a fixed current density of 50mA/cm^2. A Metrohm 691 pH meter and Metterler Toledo Inlab 730 probe were used to

measure pH value and conductivity of electrolytes, respectively. Nomination of each sample and the details about electrolyte and processing parameters were listed in Table 1. In brief, the initial capital letter "C" in the nomination system represents the constant current density power mode, while the second capital letter indicates the HAp concentration in PEO electrolyte (0-0g/L, L-5g/L, M-10g/L and H-20g/L). A magnetic stirrer was used to ensure the uniform dispersion of HA particle in the electrolyte. The temperature was maintained at 20±1 ℃ by a cooling system.

2.3 Characterization

Image analysis software ImageJ was utilized to analyze the surface porosity and average pore size from the SEM images with examined area of approximately $1mm^2$. A scanning electron microscope (Tescan Vega3) equipped with an energy dispersive X-ray spectrometer (EDS) was used for examining the surface and cross section morphology as well as element distribution of PEO coatings. For the observation of cross section, the samples were embedded into resin and then polished by emery paper with successive grades (800, 1200 and 2500) to 1μm diamond finish. Grazing incident X-ray diffraction (GIXRD, D8 Advance Bruker AXS) with Cu Kα (λ=1.54056Å) radiation at 40kV and 40mA was carried out to determine the phase composition of samples before and after immersion test. The incidence angle was 5 degree, and each scanning step was 0.05 degree for 0.5s in the range (e.g. 2θ angle) from 10 to 80 degree.

2.4 Electrochemical measurements

The electrochemical behavior was studied by electrochemical impedance spectroscopy (EIS) in simulated body fluid (SBF) using a computer controlled potentiostat system (Gamry interface 1000). The chemical composition of SBF solution was reported by Tang in detail [28]. The solution was prepared by dissolving analytical grade chemicals of NaCl (8.035g/L), $NaHCO_3$

(0.355g/L), KCl (0.225g/L), $K_2HPO_4 \cdot 3H_2O$ (0.231g/L), $MgCl_2 \cdot 6H_2O$ (0.225g/L), HCl (1mol/L, 39ml), $CaCl_2$ (0.292g/L) and Na_2SO_4 (0.072g/L) into 1L deionized water and buffered with tris-hydroxymethyl aminomethan (Tris) and 1M HCl. The final pH of SBF solution was 7.4 at 37.0 ± 0.5 ℃, and no precipitates could be observed after the solution was stabilized. A conventional three-electrode setup consisting of a working electrode (as-prepared coated samples with an exposure area of 0.5cm^2), counter electrode (a platinum spiral wire) and reference electrode (saturated Ag/AgCl) was used. EIS measurements were performed at OCP with respect to amplitude of 10 mV RMS sinusoidal perturbation over the frequency range from 10kHz to 0.1Hz. The impedance spectra were fitted using Zview software and all the measurements were repeated three times to guarantee reproducibility.

2.5 Immersion test

The long-term corrosion performance of pure Mg, Mg-PEO and Mg-PEO-HAp coatings was studied by soaking samples in SBF solution, according to ASTM G31-72 (2004). The specimens were vertically immersed in SBF solution in glass beakers, which were covered with parafilms, at 37.0 ± 0.5℃ for 7 days. The ratio of solution volume to exposed sample area was 20 ml/cm^2. After the immersion test, all samples were removed from the SBF solution and washed in deionized water, followed by drying in warm air. Again, SEM, EDS and XRD techniques were applied to characterize the microstructure, element distribution and phase composition of the soaked samples, respectively.

3 Results and discussion

3.1 Transient Voltage characteristic of PEO treatments

Fig. 2 presents the voltage transient curves in function of time for different PEO treatments without and with different concentrations of HAp. According to voltage-ramp rate, the overall process of constant current treatment can be generally divided into three consecutive stages including general passivation, spark anodization and micro arc oxidation. During stage I, from 0s to 35s, voltage of all samples increases instantaneously to 250V in a linear manner, revealing an accelerated passivation process of substrate and instant growth of the oxide layer. In addition, this sharp tendency in voltage response also implies a uniform and compact topology of the initial dielectric oxide layer, which is similar to the passivation layer formed in ambient moisture environment [25, 29]. Almost no difference could be recognized among the samples produced with the different concentrations of HAp particles. Hence, it could be expected that suspended HAp particles are not involved in the anodic passivation. As soon as the voltage reaches a critical value that is indicated by the breakdown of the dielectric layer, the treatment proceeds into the second stage (spark anodization: 35s-300s). In this stage, numerous light white sparks appear on the sample surface and shift swiftly across the surface accompanied by intensive bubble liberation. However, the voltage-ramp rate decreases significantly from 7.14 V/s in the former stage to 0.75 V/s due to the consecutive breakdown and growth of the anodized layer. It should be noted that the voltage response of samples with higher HAp concentration, especially for the CH-sample, is slightly higher than the other samples, which might result from the uptake of HA particle into PEO coatings. In the third stage (300s-600s), the light short-lived sparks gradually evolve into large and stable ones, and the color of sparks changes into dark orange, which imply the initialization of micro arc oxidation stage. The voltage increase rate for all the samples obtained in constant current mode is greatly slowed down (0.1 V/s), expiring at around 500V by the end of treatment. The similar phenomena in voltage response for all the samples indicate a

steady state, in which the growth of coating thickness is stabilized corresponding to the applied voltage.

3.2 Microstructure

Fig. 3 presents the surface morphology of PEO coatings prepared in absence and presence of various concentrations of HAp particles. Image processing (contrast identification technique) was engaged to distinguish the pores on the PEO coatings, and the analyzed results are summarized in Fig. 4. As shown, all the prepared coatings exhibit the typical surface morphology of PEO layers, characterized by micropores, microcracks and deposition of molten oxide. This traditional kind of volcano-like morphology is formed due to the ejection of molten oxide out of the discharge channels and the subsequent solidification by the electrolyte as it reaches the coating surface [30, 31]. With increasing amount of HAp particles, both the number and size of the pores on the surface tend to decrease and the surfaces become more compact. In details, the addition of 5g/L HAp does not reveal much decrease but slight increase in the surface porosity, while a dramatic decrease in the number of pore is witnessed with increasing the concentration up to 10g/L. Further increase of HAp concentration to 20g/L does not cause much further variation in the number of pores. Interestingly, the distribution of pores with respect to the size (4-7, 7-10, 10-15 and above 15 μm) reveals that smaller pores (below 10μm) take up the majority part of the overall pores and the amount of larger pores (over 10μm) is relatively low especially if HAp concentration is increasing. Obviously, HAp is beneficial to eliminating the pores on the PEO surface, and the level of such an impact is proportional to the concentration of HAp. Similar results have also been reported in previous works, in which graphite, clay as well as tungsten carbide (WC) particles are dispersed in the electrolyte for preparing PEO coatings [26, 29, 31]. So, it is reasonable to speculate that these particles may homogenize the discharge behavior,

alleviating the power of individual discharge spark and, hence, reducing the defects of the PEO coatings.

The cross-section images of coatings developed in electrolytes with different concentrations of HAp are presented in Fig. 5. The thickness of the produced coatings is measured at different regions of cross section in order to obtain an average estimation value, and the results are given in Fig 6. The thickness of C0-, CL-, CM- and CH-coating is 43.9±4.8, 36.8±1.2, 36.8±3.4 and 33.1±2.7 μm respectively, which implies that the addition and increase of HAp results in a slight decrease in the coating thickness. In terms of the morphology of cross-section, all the fabricated coatings can be divided into three different regions in general, namely outer layer, pore band and inner compact barrier layer. According to the growth mechanism reported by Hussein et al. [26, 32], PEO coatings grow towards the opposite directions simultaneously, comprising of inwards growth to the substrate and outwards growth to the coating/electrolyte interface. The inwards growth can be attributed to the diffusion of oxygen towards the Mg substrate, while the outwards increase in thickness results from the continuous ejection of molten material on the coating surface and its subsequent solidification. Eventually, the pore band is formed because the growth dynamics of the two directions are not same all the time, resulting in such an unfilled region in the coating. The outer layer is much thicker than the other two parts of the coating, taking up more than half of overall coating thickness. However, many visible defects can be observed even in a relatively low magnification. In general, these defects are residual discharge channels, entrapped gas pores and open pores, which are formed due to the short-lived sparks and spontaneous solidification caused by the instant cooling by the electrolyte. Hence, it is presumable that this outer layer cannot provide sufficient protection of substrate against corrosion. On the contrary, the inner layer is only about 2μm thick, but few defects can be revealed in the

layer and at the coating/substrate boundary. Therefore, it can be understood that the prepared coatings are cohesively attached to the substrate and resistive to corrosion mainly due to the protection of the relatively compact inner layer. Moreover, with addition and increasing the concentration of HAp particles, the defects existed in the outer layer tend to be sealed. This optimization in cross-section morphology agrees well with corresponding surface microstructure, which suggests the HAp particles could affect the discharge behavior and change the coating composition [33].

3.3 Elemental and phase composition

To further trace the suspended HAp particles and investigate the elemental composition of the obtained coatings, EDS analysis (scanned area= appr. 4mm^2) was carried out on the coating surface and the results are summarized in Table 2. Comparing to C0-coating without Ca presence, CL-, CM- and CH-coating prepared with 5, 10 and 20 g/L HAp addition reveal a Ca content of 4.6, 7.7 and 11.0 at.% respectively. The concentration of P remains almost stable while increasing concentration of HAp particles in electrolyte. These results strongly suggest a reactive incorporation mechanism of HAp into PEO coatings, in which only the amount of Ca is proportional to the concentration of suspended HAp. Fig. 7 and 8 present the EDS mapping and line scan across the thickness of CH-coating, respectively. It can be noted that P and O are uniformly distributed over the whole cross-section, while Ca shows some aggregation in the pore band (dash line). The line scan (black line: P, red line: Ca) also confirms a higher amount of Ca and P in the pore band region.

Fig.9 presents the GIXRD patterns of the different coatings and the pattern of the HAp particles. A broad bump distributing in the range of 20 to 35 degree of 2θ for all the coatings suggests the existence of amorphous phases, which are likely originated from the fast solidification process of

the ejected molten oxide. In addition, typical diffraction peaks from $Mg_3(PO_4)_2$, MgO and Mg phases are detected in the C0-coating, which is consistent with the results reported in previous work [25]. With addition of HAp particles, the $Mg_3(PO_4)_2$ phase is rarely to be found. Instead, a new calcium-deficiency phase ($Na_2CaMg_7(PO_4)_6$ Chladnite: PDF 00-047-1763) is formed.

According to our previous works [33, 34], the incorporation of particles into PEO coating is strongly dependent on the particle size and their melting temperature. Comparing with the sizes of pores on the surface of coating, most of the HAp particles are small enough to enter into the coating through the discharge channels and being deposited in the pore band of the coating. In addition to the entrapped particles, the discharge channels are also filled up with electrolyte. As soon as the breakdown of the oxide coating by the spark discharge, extreme high temperature and pressure [35] are introduced. Local melting of the substrate and coating materials together with the incorporated particles can occur simultaneously. With respect to the used HAp particle itself, a hexagonal crystalline structure (PDF 00-046-0905) was determined by XRD, which is less stable than its monoclinic alternatives [36, 37]. Combining the unstable crystal structure, small scale particle size and low melting point, it is not hard to speculate the HAp particles are possible to be molten and form a new composite phase $Na_2CaMg_7(PO_4)_6$.

3.4 Corrosion performance

3.4.1 Electrochemical impedance spectroscopy (EIS)

Electrochemical impedance spectroscopy (EIS) was employed to characterize the corrosion and degradation process of coatings in SBF solution at 37.0 ± 0.5 ℃ up to 72 hours. The Nyquist and Bode plots in Fig. 10 compare the respective response of the four PEO coatings after different immersion times (1, 12, 24, 48 and 72h). At the beginning, after 1h stabilization in SBF solution,

all the coatings display a double-loop pattern in Nyquist plot, which coincides well with their respective curves in Bode plot at middle and low frequencies. Closer look to the Bode plots shows that at high frequencies there are certain signs of a third relaxation process. This high-frequency time constant can be associated to the response of the outer PEO layer, while the one at middle frequencies describe the response from the inner barrier layer. Finally, the low-frequency relaxation process can be assigned to the electrochemical activity (double layer capacitance and charge transfer resistance) in the defects at metal/electrolyte interface. Addition of HAp to the PEO electrolyte remarkably increases the total impedance of some coatings even at initial immersion stages. However, this effect becomes even more evident in course of immersion. The blank PEO coating demonstrates only a moderate increase of the impedance values at low frequencies while the systems with particles exhibit much more remarkable effect achieving sometimes almost 10 folds higher values after 72 hours when compared to the initial impedance. Closer look to the evolution of impedance spectra suggests possible explanation of this phenomenon. There is an important increase of the pore resistance of outer layer, resistive impedance response at about 1000Hz, with immersion time for the coatings which contain particles. The high frequency time constant becomes more evident with time in the case HAp-containing coatings in contrast to the blank one. Such a behavior suggests that there is an important sealing of the outer layer by a kind of insoluble conversion products formed in the open pores as a result of corrosion process or/and transformation of coating components during immersion in SBF. The evolution of middle frequency capacitive response related to the capacitance of inner barrier layer is also significantly affected by the presence of HAp in the coatings. The particle free system demonstrates quite stable values in course of immersion, while the CL-, CM-, and CH- coatings show a remarkable decrease of the capacitance. Such a decrease can be assigned to increase of the barrier thickness or to a decrease of the surface area of carrier

layer exposed to the electrolyte through the pores in the outer layer. Both these factors occurring at the same time can also play a role.

The equivalent circuit schematically shown in Fig.11 has been used in this work to fit the experimental spectra and quantify the important physicochemical parameters describing the evolution of respective coatings. In the proposed circuit, R_s stands for resistance of electrolyte between working electrode and reference electrode. Two consecutive groups of paralleled combination of resistor (R_o and R_i) and constant phase element (CPE_o and CPE_i) are applied to describe the resistance and capacitance of the outer porous and inner barrier layer, respectively. R_{ct} and CPE_{dl} represent the charge transfer resistance and electrochemical double layer capacitor at the substrate/coating interface, whereas R_0 and CPE_o imply the resistive and capacitive response from the outer porous layer. The constant phase elements are used here instead of capacitances in order to account for non-uniform distribution of parameters. Fitted curves are given as solid lines shown in Nyquist and Bode graphs (Fig. 10). Note, Chi-squared is used as an index to evaluate the goodness of fitting, and this value is less than 10^{-3} for all current fitting, which confirms an acceptable error.

For a comprehensive understanding of the degradation of the studied coatings, the evolution of the resistance of different layers, including R_o, R_i, R_{ct} as well as R_{sum}, is illustrated in Fig. 12. The resistance of the outer layer always shows the lowest values in comparison to the contribution of other components. It is caused by the highly porous nature of this layer as a result of discharges which leaves pores going through the outer layer and creates the pore band. Only a minimal difference in this parameter for all the samples can be distinguished at the test. All the samples with HAp addition in the electrolyte show a well-defined increasing trend during 72h, while the bare PEO specimen remains at a relative low value. Importantly the increase of the particle

concentration in the electrolyte generally leads to stronger effect. According to the conclusion drawn in reference [38, 39], the presence of hydroxyapatite layer in the coating could trigger the nucleation and deposition of calcium phosphate (e.g. apatite), which in turn enhances the resistance of the outer layer. Therefore, the coating with more HAp addition reveals higher resistance in the outer layer. The resistance of inner layer for each coating is one or two orders higher than that of the outer layer taking up the majority resistance of the whole coating. Moreover, the CL-, CM- and CH-coating receive an increase in R_i values, which is proportional to the concentration of added HA particles. As discussed above the thickening of the inner barrier layer, sealing of the defects in such a layer by precipitates or reducing the surface area of the inner layer exposed to the electrolyte in pores can be responsible this increase. As the enhancement of R_i, the charge transfer resistance (R_{ct}) shows the similar tendency, in which the increase of each sample corresponds to HAp concentration. As discussed before, the increase in R_i and R_{ct} results from sealing of the inner porosity and defects by the incubated precipitation of corrosion products at local corroded spots. It should also be noted that, in addition to the Ca/P composition of PEO-HAp, the optimization of microstructure can also facilitate the enhancement of resistance. As shown in Fig. 3, the addition of HAp particles relieves the porosity in the coating, impeding the penetration of electrolyte. Overall, with consideration of composition and structure, CH-coating produced with 20g/L HAp addition reveals a higher corrosion resistance throughout 72h immersion.

3.4.2 Immersion test

The long-term corrosion response and ability for inducing the precipitation of HAp on coating from SBF solution of the obtained PEO coatings are evaluated by immersion test. Fig. 13 compares the surface morphologies of bare magnesium and PEO coated specimens after 7d

immersion in neutral SBF solution at 37.0 ± 0.5 °C. After drying, a uniform degradation can be observed on the bulk Mg substrate, which is characterized by numerous cracks and debris on the surface. In principal, Mg can be oxidized into Mg^{2+} ions by H_2O molecule in ambient environment, releasing H_2 and depositing $Mg(OH)_2$ precipitates on the sample surface (see Equation (1) and (2) [1, 2]). As the dehydration of $Mg(OH)_2$, according to Equation (3), the volume of pre-deposited hydroxide layer possesses a tendency to shrink, resulting in the aforementioned cracks and peeling-offs on the Mg surface.

$$2Mg + 2H_2O \rightarrow 2Mg^{2+} + 2OH^- + H_2 \quad (1)$$

$$Mg^{2+} + 2OH^- \rightarrow Mg(OH)_2 \quad (2)$$

$$Mg(OH)_2 \rightarrow MgO + H_2O \quad (3)$$

For the PEO-coated samples (Fig. 13 (b-e)), on the other hand, the surfaces just reveal a slight degradation in comparison with those before immersion. This variation in surface morphology is closely related with the degradation of PEO coating, during which the hidden closed pores are gradually exposed to the electrolyte. This is because of MgO, the main composition of PEO coating, is not stable in aqueous environment [1], and facilitates the reaction in Equation (3) proceeding towards the adverse direction. Consequently, the PEO coatings also show slight degradation as indicated by the increasing amount and enlargement of the micropores on the surfaces, since the degradation always initializes from these defects. On the other hand, it should be also noted that the corrosion products and precipitates are more favorable to be deposited along or even inside these defects (cracks and pores), where the nucleation is easier than at the smooth regions. Since the calcium phosphate is able to nucleate both in the SBF solution and on the metal surface simultaneously [40], this precipitates on the sample surface is suggested to be the CaP compounds. The defects in coatings are gradually sealed by the precipitates and

accumulation of corrosion products, and this could partially contribute to the consecutive increase in the coating impedance (Fig. 10).

Fig.14 and Fig. 15 show the variation in atomic Ca/P ratio and phase composition of the immersed samples, respectively. After 7 days immersion, the atomic Ca/P ratio receives an increase for all the test samples. Bare Mg shows the greatest promotion of 0.7 in this value, which confirms the deposition of Ca^{2+} and HPO_4^{2-} ions onto the surface, since the local alkaline environment caused by the corrosion of Mg favors this action. Nevertheless, instead of any crystalline CaP compound(s), most of the corrosion produces are nano-crystalline or amorphous phases for the corroded Mg sample, which are characterized by the wide bumps distributed in the lower degree range. According to Cao and Pamela Habibovic et al., Mg^{2+} kinetically hinders the nucleation and subsequent growth of HAp through competing the molecule structural sites with Ca^{2+} [40-43]. When the concentration of Mg^{2+} is below 35 atomic percentage, the growth of crystal is inhibited, and above this value, the precipitates are completely amorphous [44]. Hence, the presence of amorphous phase indicates a fast corrosion process (more than 35 atomic percentage Mg^{2+} is released on the surface) of bulk Mg substrate in SBF solution. On the contrary, C0-, CL- and CM-coatings just reveal some minor changes in phase composition, which indicates the stability of the fabricated coatings. In specific, $Mg_3Ca_3(PO_4)_4$ (Stanfieldite, PDF 01-073-1182) and $Ca_{9.74}(PO_4)_6(OH)_{2.08}$ (Hydroxyapatite, PDF 01-086-1199) are detected on the CH-coating with higher amount of Ca. The introduction of new phases demonstrates that Na^+ and a part of Mg^{2+} in $Na_2CaMg_7(PO_4)_6$ are substituted by Ca^{2+} from either the amorphous phase of the coating or SBF solution. Obviously, the higher percentage of Ca in the coating facilitates this transformation, and the newly introduced substance is possible to seal the pores in the coating, resulting in increasing impedance as discussed before. In short, incorporating HAp particles into PEO coating would enhance the corrosion properties of the coating, and the production of HAp

through immersion approach is achievable for PEO coating containing a relatively higher content of Ca^{2+}, which is introduced by the addition of 20g/L HAp particles in the electrolyte.

4 Conclusions

In present work PEO coatings were fabricated on Mg substrate in alkaline phosphate electrolyte with hydroxyapatite (HAp) particles addition. The influence of HAp concentration on voltage-current response, coating morphologies, composition and corrosion performance was investigated. Based on the obtained results, the following conclusion can be drawn:

(1) Considering the physical and chemical properties, HAp particles tend to be reactively incorporated into the PEO coatings during spark discharge stage producing a calcium-deficiency phase ($Na_2CaMg_7(PO_4)_6$ as a main component. Moreover, addition of HAp into electrolyte decreases the thickness and porosity of the coating, resulting in a more compact morphology and, in turn, enhanced corrosion resistance.

(2) After the initial slight degradation of the outer layer corrosion resistance (R_o), a continuous increase is observed for all the resistances used for fitting the multi-layer PEO-HAp coatings. The incorporated HAp particles improve the compactness of PEO coating, and incur the precipitation of corrosion products from the electrolyte onto the coating surface and in the coating pores. Moreover, the corrosion products produced in the pores also promote the corrosion resistance of the inner layer.

(3) During long-term immersion, PEO coatings in absence and presence of HAp demonstrate less degradation than the pure Mg substrate. Hydroxyapatite is only formed on CH-coating with 20g/L HA addition into the electrolyte, which may result from the gradual substitution of Na^+ and Mg^{2+} by Ca^{2+} in lattice structure of $(Na_2CaMg_7(PO_4)_6$. However, Mg-containing HAp

phase is still detectable after immersion in SBF solution because of the inhibition of crystallization of HAp by Mg^{2+} released from corrosion.

Acknowledgements

The technical support of Mr. Volker Heitmann and Mr. Ulrich Burmester during this work is gratefully acknowledged. Junjie Yang thanks China Scholarship Council for the award of fellowship and funding.

Reference:

[1] G. Song, A. Atrens, Understanding Magnesium Corrosion—A Framework for Improved Alloy Performance, Adv. Eng. Mater, 5 (2003) 837-858.

[2] G.L. Song, A. Atrens, Corrosion mechanisms of magnesium alloys, Adv Eng Mater, 1 (1999) 11-33.

[3] F. Witte, Reprint of: The history of biodegradable magnesium implants: A review, Acta. Biomater, 23 Suppl (2015) S28-40.

[4] A.H. Martinez Sanchez, B.J.C. Luthringer, F. Feyerabend, R. Willumeit, Mg and Mg alloys: how comparable are in vitro and in vivo corrosion rates- A review, Acta. Biomater, 13 (2015) 16-31.

[5] M.P. Staiger, A.M. Pietak, J. Huadmai, G. Dias, Magnesium and its alloys as orthopedic biomaterials: A review, Biomater, 27 (2006) 1728-1734.

[6] R.I.M. Asri, W.S.W. Harun, M.A. Hassan, S.A.C. Ghani, Z. Buyong, A review of hydroxyapatite-based coating techniques: Sol-gel and electrochemical depositions on biocompatible metals, J. Mech. Behave. Biomed, 57 (2016) 95-108.

[7] Y.L. Kuo, K.H. Chang, Atmospheric pressure plasma enhanced chemical vapor deposition of SiOx films for improved corrosion resistant properties of AZ31 magnesium alloys, Surf. Coat. Tech, 283 (2015) 194-200.

[8] J.F. Ou, W.H. Hu, M.S. Xue, F.J. Wang, W. Li, Superhydrophobic Surfaces on Light Alloy Substrates Fabricated by a Versatile Process and Their Corrosion Protection, Acs. Appl. Mater. Inter, 5 (2013) 3101-3107.

[9] Y. Song, S.X. Zhang, J.A. Li, C.L. Zhao, X.N. Zhang, Electrodeposition of Ca-P coatings on biodegradable Mg alloy: In vitro biomineralization behavior, Acta. Biomater, 6 (2010) 1736-1742.

[10] A.R. Vaccaro, The role of the osteoconductive scaffold in synthetic bone graft, Orthopedics, 25 (2002) S571-S578.

[11] J.M. Lane, A.W. Yasko, E. Tomin, B.J. Cole, S. Waller, M. Browne, T. Turek, J. Gross, Bone Marrow and Recombinant Human Bone Morphogenetic Protein-2 in Osseous Repair, Clin. Orthop. Relat R, 361 (1999) 216-227.

[12] G.Y. Liu, J. Hu, Z.K. Ding, C. Wang, Bioactive calcium phosphate coating formed on micro-arc oxidized magnesium by chemical deposition, Appl. Surf. Sci, 257 (2011) 2051-2057.

[13] V. Kaesel, P.T. Tai, F.W. Bach, H. Haferkamp, F. Witte, H. Windhagen, Approach to Control the Corrosion of Magnesium by Alloying, Magnesium, Wiley-VCH Verlag GmbH & Co. KGaA2005, pp. 534-539.

[14] L. Bakhtiari, H.R. Rezaie, S.M. Hosseinalipour, M.A. Shokrgozar, Investigation of biphasic calcium phosphate/gelatin nanocomposite scaffolds as a bone tissue engineering, Ceram. Int, 36 (2010) 2421-2426.

[15] A. Seyfoori, S. Mirdamadi, Z.S. Seyedraoufi, A. Khavandi, M. Aliofkhazraei, Synthesis of biphasic calcium phosphate containing nanostructured films by micro arc oxidation on magnesium alloy, Mater. Chem. Phys, 142 (2013) 87-94.

[16] K.J. Quelch, R.A. Melick, P.J. Bingham, S.M. Mercuri, Chemical composition of human bone, Arch. Oral. Biol, 28 (1983) 665-674.

[17] H. Tang, Y. Gao, Preparation and characterization of hydroxyapatite containing coating on AZ31 magnesium alloy by micro-arc oxidation, J. Alloy. Compd., 688, Part A (2016) 699-708.

[18] S.V. Gnedenkov, Y.P. Sharkeev, S.L. Sinebryukhov, O.A. Khrisanfova, E.V. Legostaeva, A.G. Zavidnaya, A.V. Puz, I.A. Khlusov, D.P. Opra, Functional coatings formed on the titanium and magnesium alloys as implant materials by plasma electrolytic oxidation technology: fundamental principles and synthesis conditions, Corr. Rev, 34 (2016) 65-83.

[19] S.V. Gnedenkov, S.L. Sinebryukhov, A.G. Zavidnaya, V.S. Egorkin, A.V. Puz, D.V. Mashtalyar, V.I. Sergienko, A.L. Yerokhin, A. Matthews, Composite hydroxyapatite–PTFE coatings on Mg–Mn–Ce alloy for resorbable implant applications via a plasma electrolytic oxidation-based route, J. Taiwan. Inst. Chem. E, 45 (2014) 3104-3109.

[20] G.Y. Liu, J. Hu, Z.K. Ding, C. Wang, Formation mechanism of calcium phosphate coating on micro-arc oxidized magnesium, Mater. Chem. Phys, 130 (2011) 1118-1124.

[21] Y. Gao, A. Yerokhin, A. Matthews, Deposition and evaluation of duplex hydroxyapatite and plasma electrolytic oxidation coatings on magnesium, Surf. Coat. Tech, 269 (2015) 170-182.
[22] Y. Wang, D.B. Wei, J. Yu, S.C. Di, Effects of Al2O3 Nano-additive on Performance of Micro-arc Oxidation Coatings Formed on AZ91D Mg Alloy, J. Mater. Sci. Technol., 30 (2014) 984-990.
[23] Y.L. Song, X.Y. Sun, Y.H. Liu, Effect of TiO 2 nanoparticles on the microstructure and corrosion behavior of MAO coatings on magnesium alloy, Mater. Corros, 63 (2012) 813-818.
[24] T.S. Lim, H.S. Ryu, S.-H. Hong, Electrochemical corrosion properties of CeO2-containing coatings on AZ31 magnesium alloys prepared by plasma electrolytic oxidation, Corros. Sci, 62 (2012) 104-111.
[25] K.M. Lee, K.R. Shin, S. Namgung, B. Yoo, D.H. Shin, Electrochemical response of ZrO2-incorporated oxide layer on AZ91 Mg alloy processed by plasma electrolytic oxidation, Surf. Coat. Tech, 205 (2011) 3779-3784.
[26] X.P. Lu, S.P. Sah, N. Scharnagl, M. Stormer, M. Starykevich, M. Mohedano, C. Blawert, M.L. Zheludkevich, K.U. Kainer, Degradation behavior of PEO coating on AM50 magnesium alloy produced from electrolytes with clay particle addition, Surf. Coat. Tech, 269 (2015) 155-169.
[27] X.P. Lu, M. Mohedano, C. Blawert, E. Matykina, R. Arrabal, K.U. Kainer, M.L. Zheludkevich, Plasma electrolytic oxidation coatings with particle additions - A review, Surf. Coat. Tech, 307 (2016) 1165-1182.
[28] H. Tang, D.Z. Yu, Y. Luo, F.P. Wang, Preparation and characterization of HA microflowers coating on AZ31 magnesium alloy by micro-arc oxidation and a solution treatment, Appl. Surf. Sci, 264 (2013) 816-822.
[29] H. NasiriVatan, R. Ebrahimi-Kahrizsangi, M.K. Asgarani, Tribological performance of PEO-WC nanocomposite coating on Mg Alloys deposited by Plasma Electrolytic Oxidation, Tribol. Int., 98 (2016) 253-260.
[30] H. Duan, K. Du, C. Yan, F. Wang, Electrochemical corrosion behavior of composite coatings of sealed MAO film on magnesium alloy AZ91D, Electrochim. Acta, 51 (2006) 2898-2908.
[31] B. Yin, Z.J. Peng, J. Liang, K.J. Jin, S.Y. Zhu, J. Yang, Z.H. Qiao, Tribological behavior and mechanism of self-lubricating wear-resistant composite coatings fabricated by one-step plasma electrolytic oxidation, Tribol. Int., 97 (2016) 97-107.
[32] R.O. Hussein, X. Nie, D.O. Northwood, An investigation of ceramic coating growth mechanisms in plasma electrolytic oxidation (PEO) processing, Electrochim. Acta, 112 (2013) 111-119.
[33] X.P. Lu, C. Blawert, Y.D. Huang, H. Ovri, M.L. Zheludkevich, K.U. Kainer, Plasma electrolytic oxidation coatings on Mg alloy with addition of SiO2 particles, Electrochim. Acta, 187 (2016) 20-33.
[34] X.P. Lu, C. Blawert, K.U. Kainer, M.L. Zheludkevich, Investigation of the formation mechanisms of plasma electrolytic oxidation coatings on Mg alloy AM50 using particles, Electrochim. Acta, 196 (2016) 680-691.
[35] R.O. Hussein, X. Nie, D.O. Northwood, A. Yerokhin, A. Matthews, Spectroscopic study of electrolytic plasma and discharging behaviour during the plasma electrolytic oxidation (PEO) process, J Phy. D. Appl. Phys, 43 (2010).
[36] S. Raynaud, E. Champion, D. Bernache-Assollant, P. Thomas, Calcium phosphate apatites with variable Ca/P atomic ratio I. Synthesis, characterisation and thermal stability of powders, Biomater, 23 (2002) 1065-1072.
[37] G. Ma, X.Y. Liu, Hydroxyapatite: Hexagonal or Monoclinic, Crys. Growth. Des, 9 (2009) 2991-2994.
[38] M. Sowa, J. Worek, G. Dercz, D.M. Korotin, A.I. Kukharenko, E.Z. Kurmaev, S.O. Cholakh, M. Basiaga, W. Simka, Surface characterisation and corrosion behaviour of niobium treated in a Ca- and P-containing solution under sparking conditions, Electrochim. Acta, 198 (2016) 91-103.
[39] W.K. Yeung, I.V. Sukhorukova, D.V. Shtansky, E.A. Levashov, I.Y. Zhitnyak, N.A. Gloushankova, P.V. Kiryukhantsev-Korneev, M.I. Petrzhik, A. Matthews, A. Yerokhin, Characteristics and in vitro response of thin hydroxyapatite-titania films produced by plasma electrolytic oxidation of Ti alloys in electrolytes with particle additions, RSC Adv., 6 (2016) 12688-12698.
[40] P. Habibovic, F. Barrere, C.A. van Blitterswijk, K. de Groot, P. Layrolle, Biomimetic hydroxyapatite coating on metal implants, J. Am. Ceram Soc, 85 (2002) 517-522.

[41] Y. Wang, M. Wei, J. Gao, J. Hu, Y. Zhang, Corrosion process of pure magnesium in simulated body fluid, Mater. Lett., 62 (2008) 2181-2184.
[42] W. Kibalczyc, J. Christoffersen, M.R. Christoffersen, A. Zielenkiewicz, W. Zielenkiewicz, The effect of magnesium ions on the precipitation of calcium phosphates, J. Cryst. Growth, 106 (1990) 355-366.
[43] X.D. Cao, W. Harris, Carbonate and magnesium interactive effect on calcium phosphate precipitation, Environ. Sci. Technol, 42 (2008) 436-442.
[44] A. Bigi, G. Falini, E. Foresti, A. Ripamonti, M. Gazzano, N. Roveri, Magnesium influence on hydroxyapatite crystallization, J. Inorg. Biochem, 49 (1993) 69-78.

Fig. 1 SEM image of HAp particles

Fig. 2 Potential transient curves during PEO treatments

Fig. 3 Surface morphology of PEO coatings with and without HAp
(a) C0-, (b) CM-, (c) CL- and (d) CH-coating

Fig. 4 Surface porosity analysis for PEO coatings ($1mm^2$) in absence and presence of HAp particles

Fig. 5 Cross-section morphology of PEO coatings without and with HA addition
(a) C0-, (b) CM-, (c) CL- and (d) CH-coating

Fig. 6 Thickness of PEO coatings in absence and presence of HA

Fig. 7 EDS mapping of CH-coating

Fig. 8 EDS line-scan of CH-coating

Fig. 9 GIXRD patterns in 5 ° grazing angle for PEO coatings without and with different concentrations of HAp

Fig. 10 Nyquist and bode plots for PEO coatings after different immersion duration

(a)(b)C0-, (c)(d) CL-, (e)(f) CM- and (g)(h) CH-coating

Fig. 11 Equivalent circuit for simulating the corrosion process of PEO coatings

Fig. 12 The variation in impedance of different layers and sum impedance during 72h immersion (a) R_o; (b) R_i; (c) R_{ct} and (d) R_{sum}

Fig. 13 Surface morphology after immersion in SBF solution for 7 day at 36±0.5℃

(a) hp-Mg, (b) C0-, (c) CL-, (d) CM- and (e) CH-coating

Fig. 14 Ca/P ratio before and after immersion test

Fig. 15 GIXRD patterns for PEO samples after 7d immersion

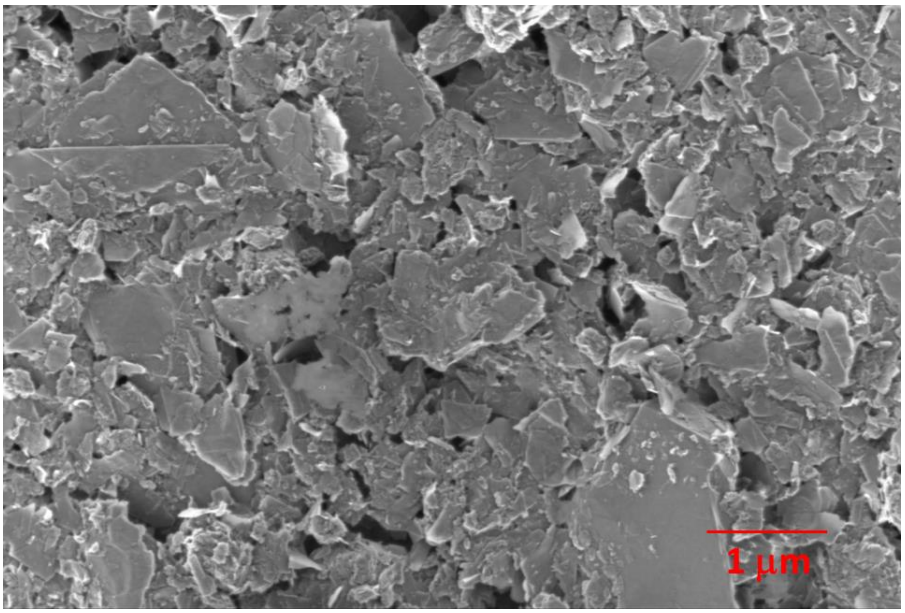
1 μm
Fig. 1

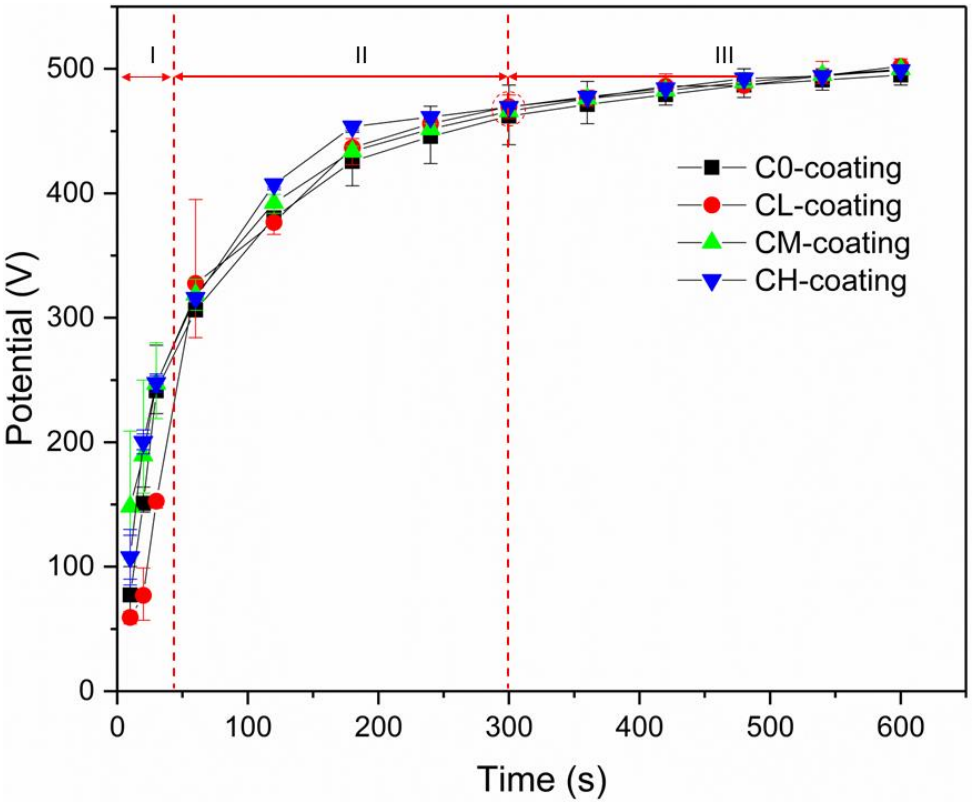
I
II
III
C0-coating
CL-coating
CM-coating
CH-coating
Potential (V)
Time (s)
0
100
200
300
400
500
600
Fig. 2

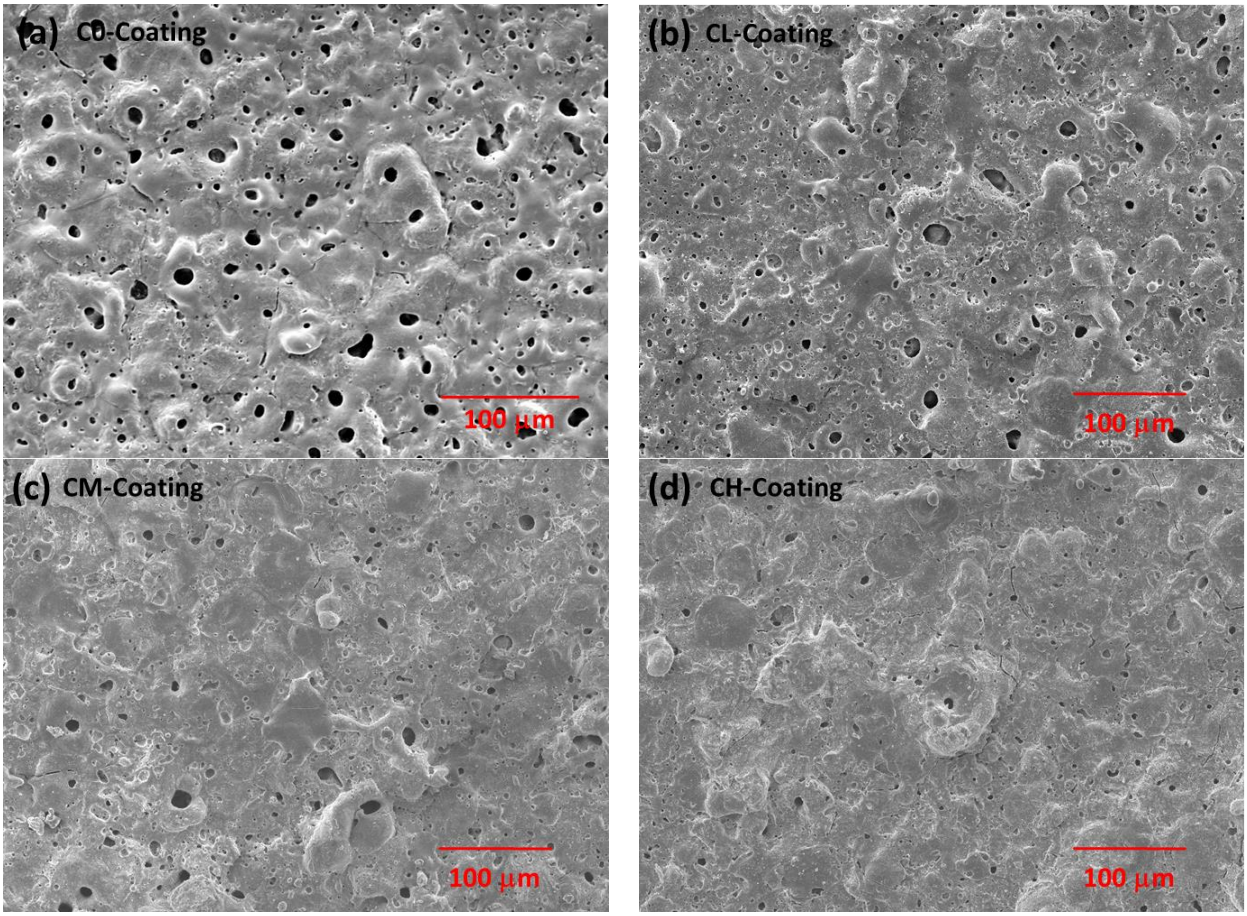
(a) C0-Coating
100 μm
(b) CL-Coating
100 μm
(c) CM-Coating
100 μm
(d) CH-Coating
100 μm

Fig. 3

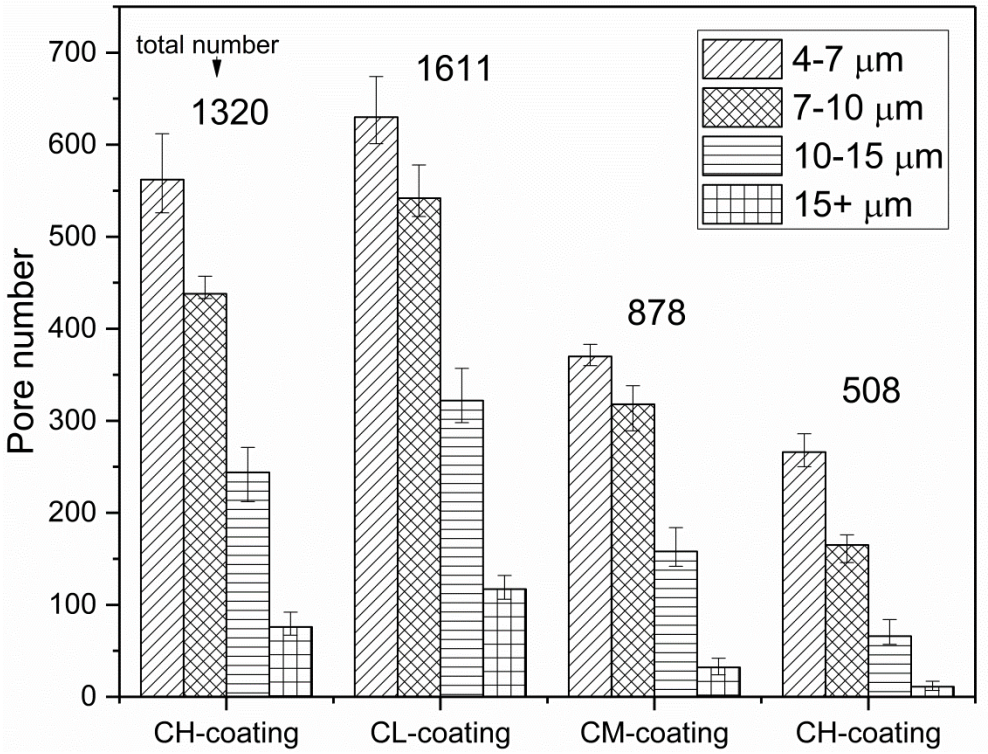
total number
1320
1611
878
508
4-7 μm
7-10 μm
10-15 μm
15+ μm
Pore number
0
100
200
300
400
500
600
700
CH-coating
CL-coating
CM-coating
CH-coating
Fig. 4

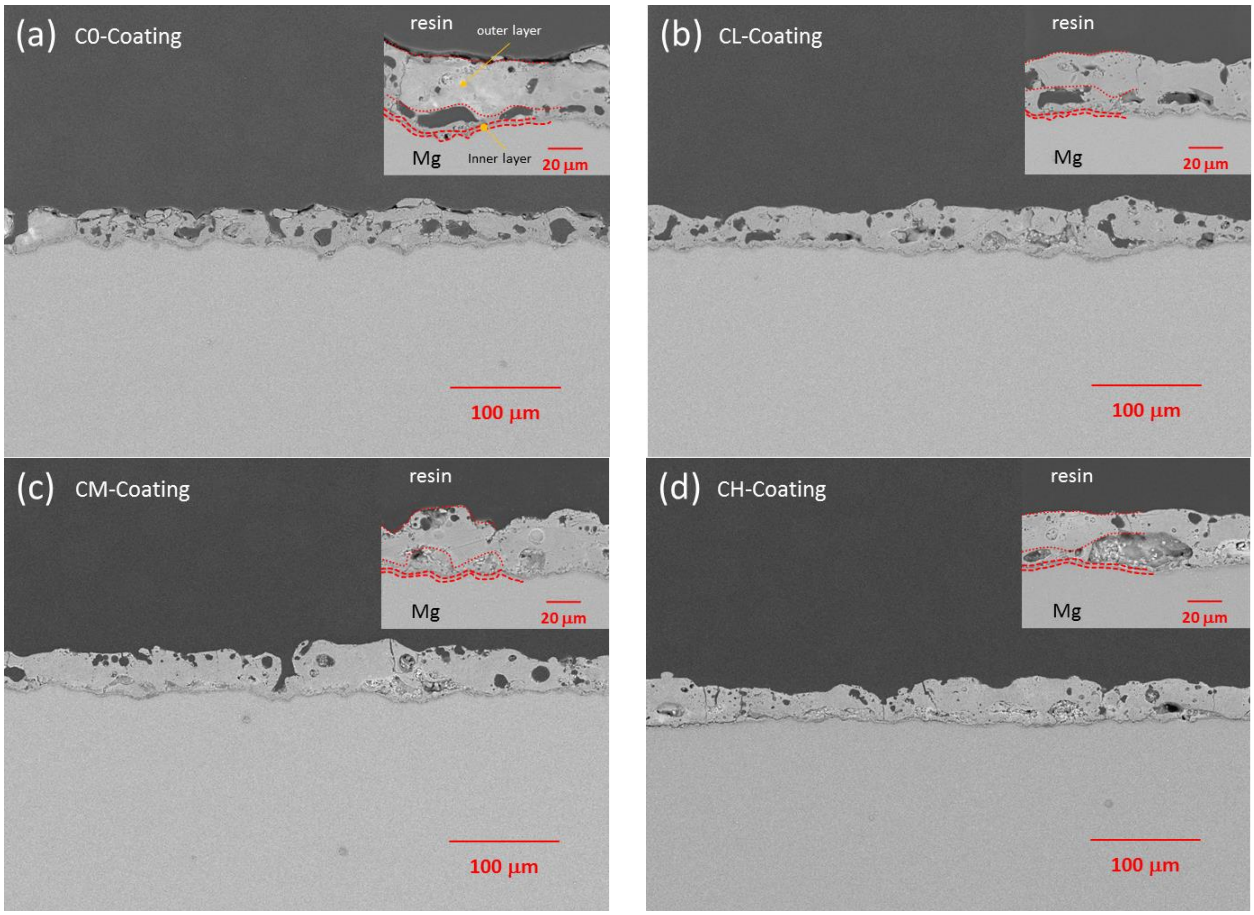
(a) C0-Coating
resin
outer layer
Mg
Inner layer
20 μm
100 μm
(b) CL-Coating
resin
Mg
20 μm
100 μm
(c) CM-Coating
resin
Mg
20 μm
100 μm
(d) CH-Coating
resin
Mg
20 μm
100 μm

Fig. 5

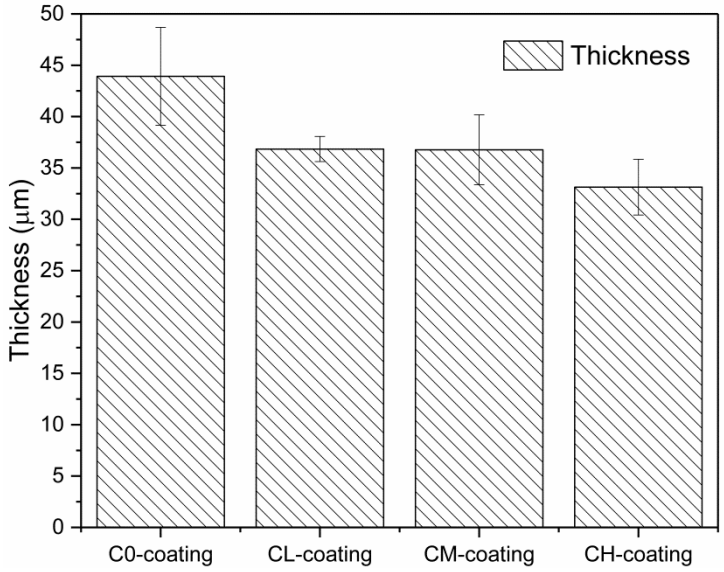
Thickness
Thickness (μm)
50
45
40
35
30
25
20
15
10
5
0
C0-coating
CL-coating
CM-coating
CH-coating

Fig. 6

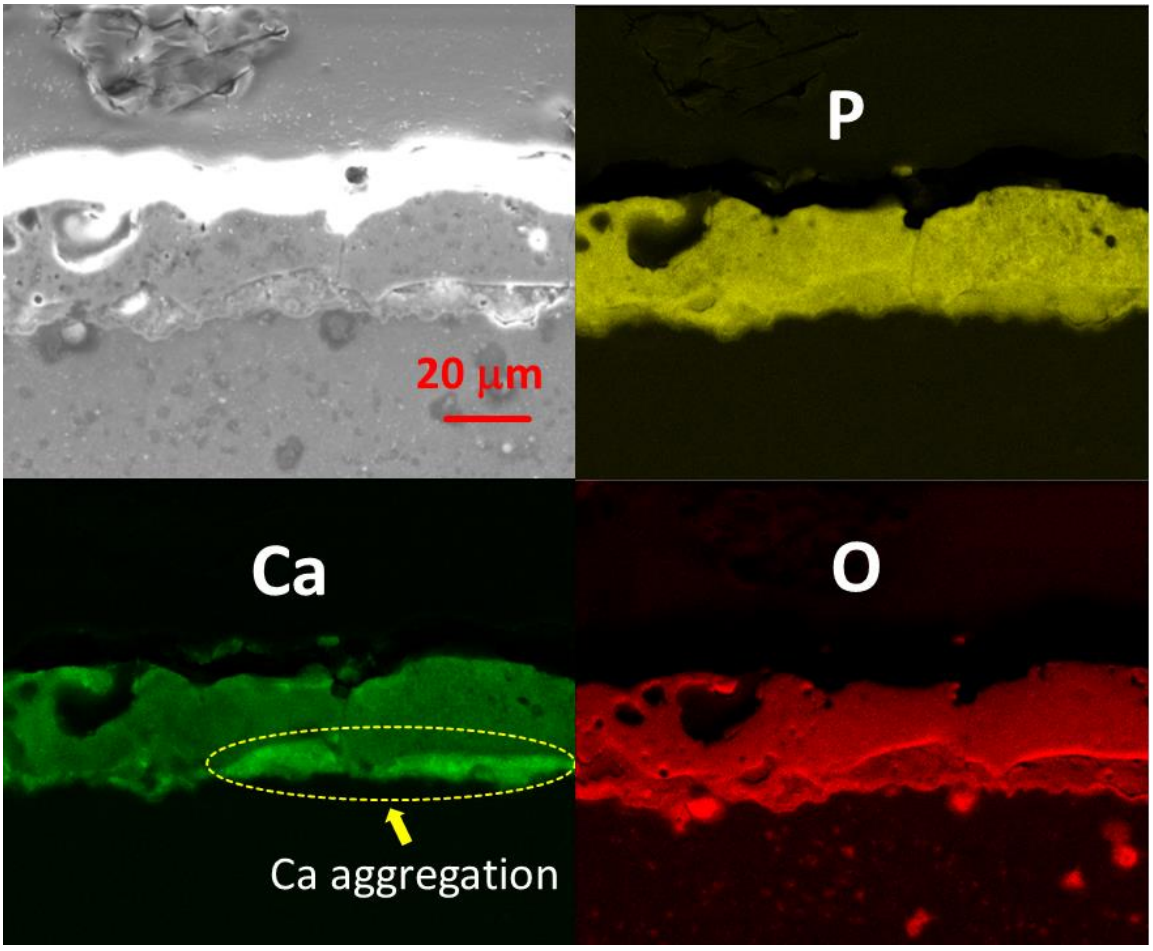
20 μm
P
Ca
O
Ca aggregation

Fig. 7

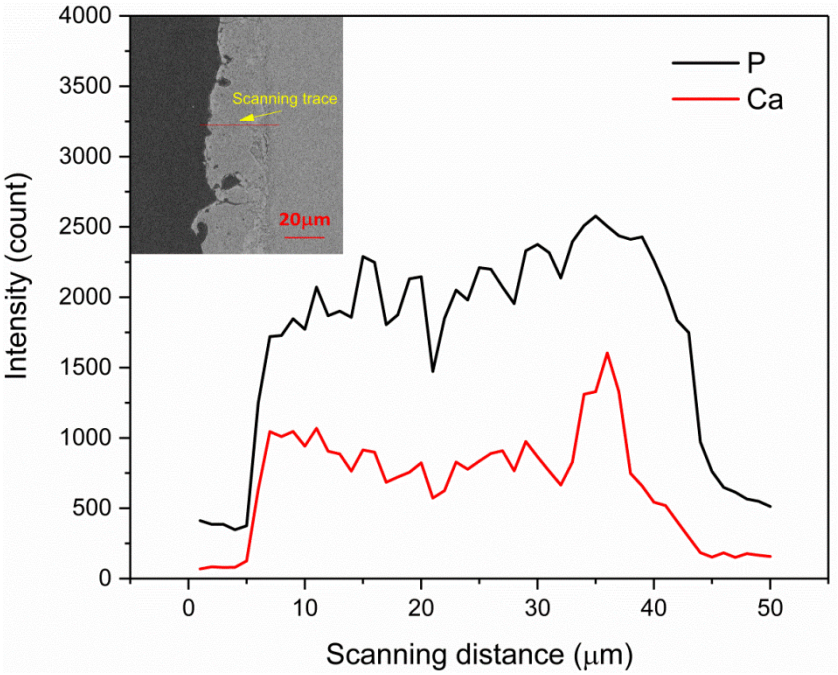
Intensity (count)
Scanning distance (μm)
P
Ca
Scanning trace
20μm
0
500
1000
1500
2000
2500
3000
3500
4000
0
10
20
30
40
50

Fig. 8

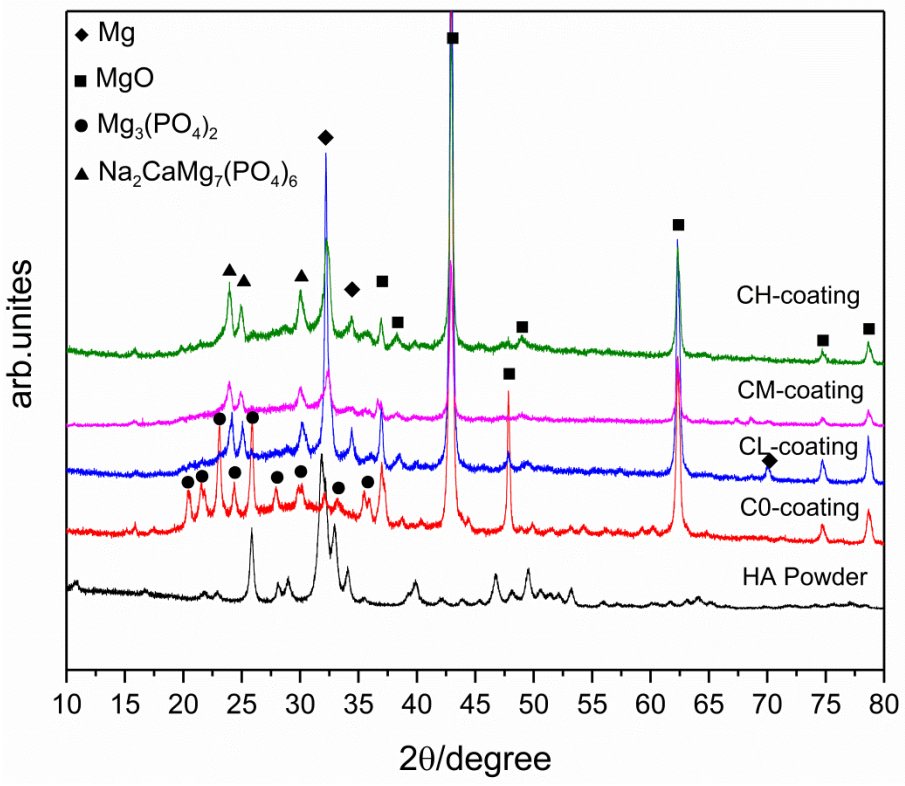
Mg
MgO
Mg3(PO4)2
Na2CaMg7(PO4)6
arb.unites
2θ/degree
CH-coating
CM-coating
CL-coating
C0-coating
HA Powder
10
15
20
25
30
35
40
45
50
55
60
65
70
75
80

Fig. 9

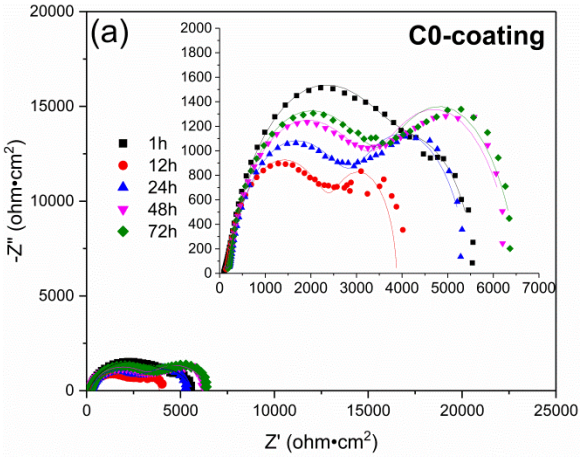
(a)
C0-coating
1h
12h
24h
48h
72h
-Z'' (ohm•cm2)
Z' (ohm•cm2)

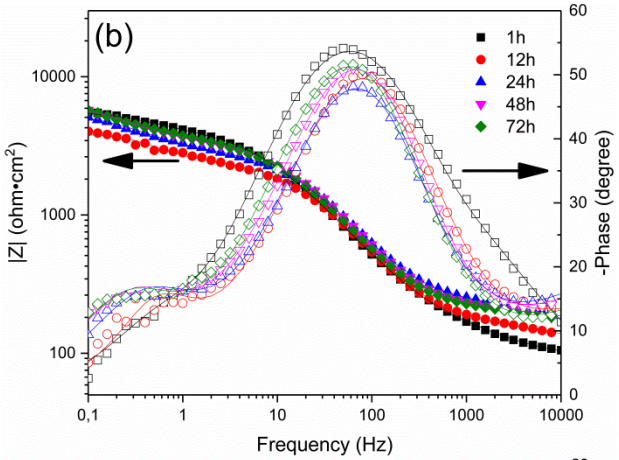
(b)
1h
12h
24h
48h
72h
|Z| (ohm•cm2)
-Phase (degree)
Frequency (Hz)

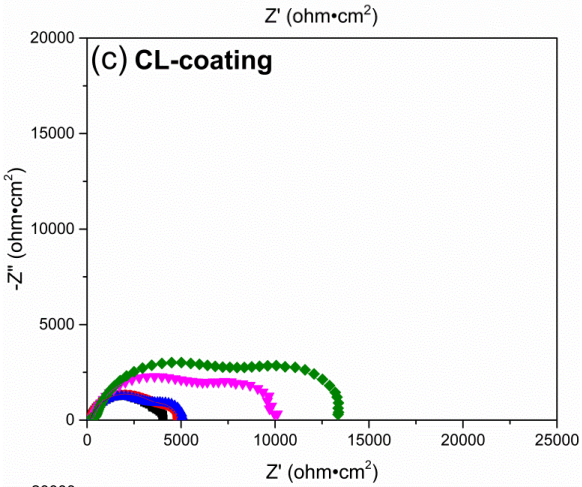
(c) CL-coating
-Z'' (ohm•cm2)
Z' (ohm•cm2)

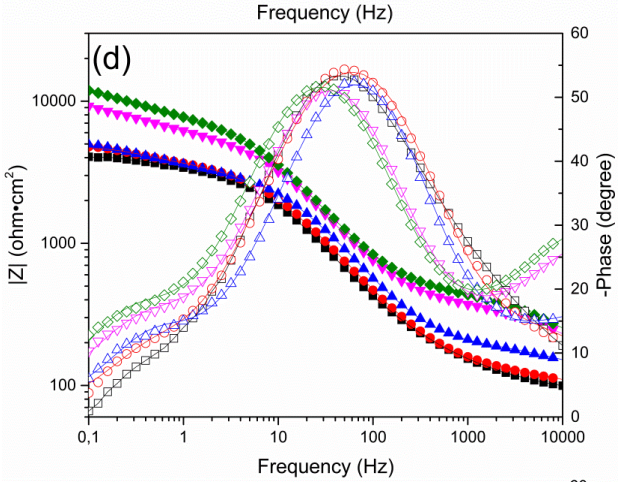
(d)
|Z| (ohm•cm2)
-Phase (degree)
Frequency (Hz)

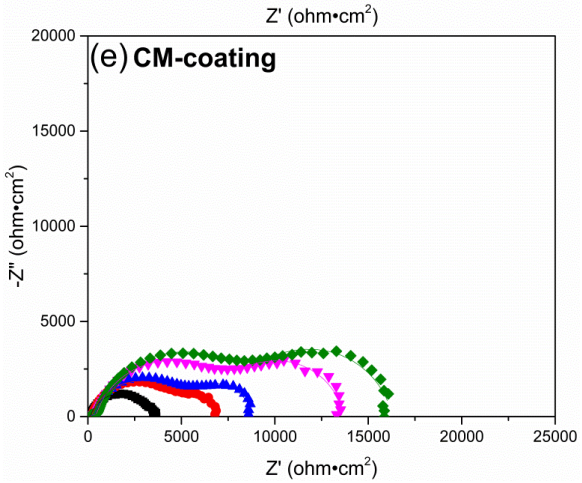
(e) CM-coating
-Z'' (ohm•cm2)
Z' (ohm•cm2)

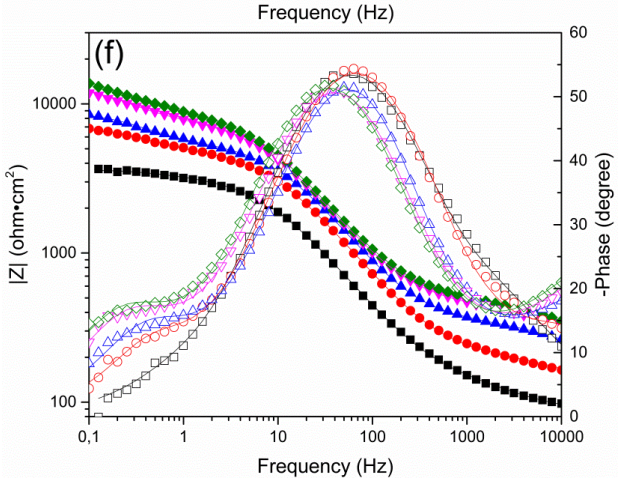
(f)
|Z| (ohm•cm2)
-Phase (degree)
Frequency (Hz)

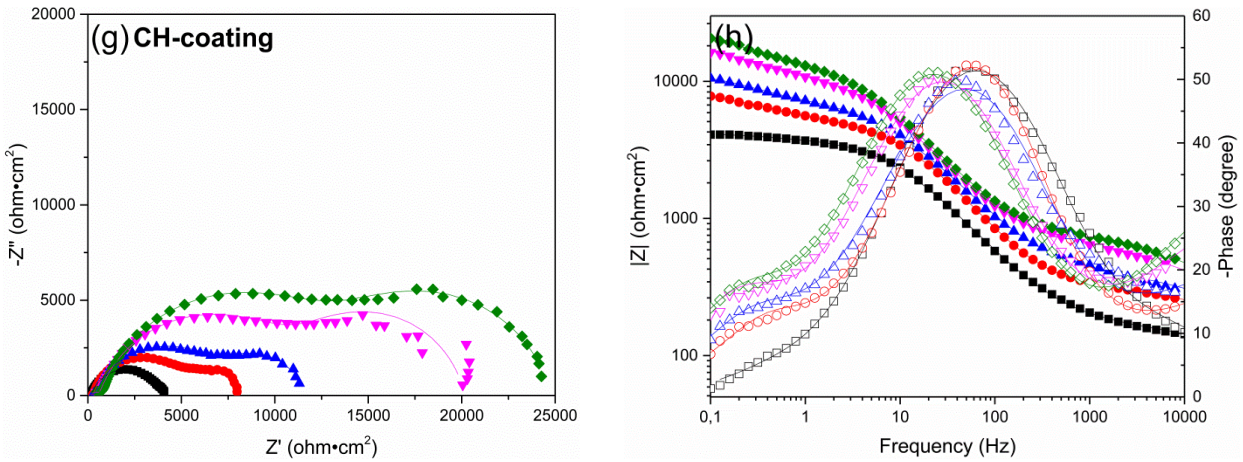
(g) CH-coating
-Z'' (ohm•cm²)
Z' (ohm•cm²)
(h)
|Z| (ohm•cm²)
-Phase (degree)
Frequency (Hz)

Fig. 10

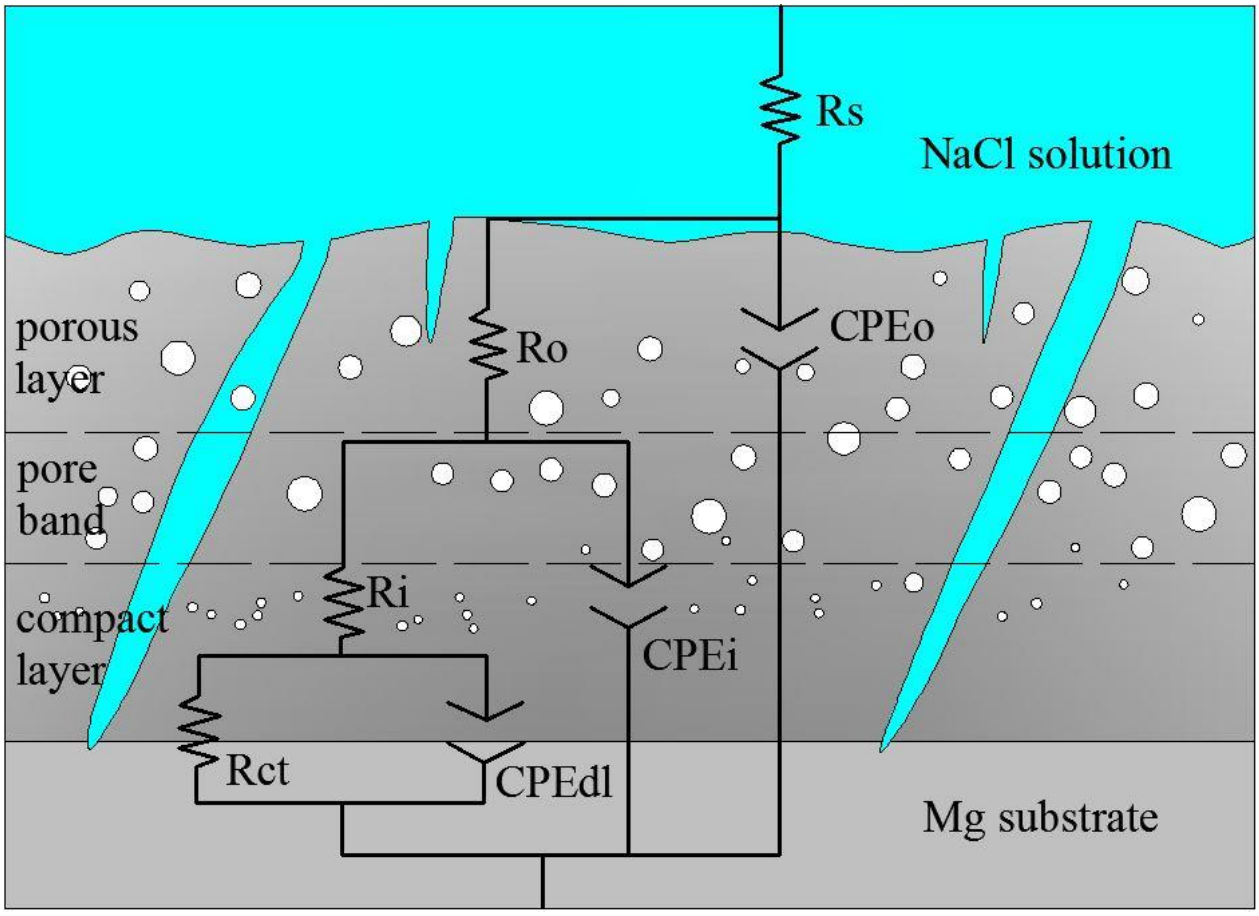
Rs
NaCl solution
porous layer
Ro
CPEo
pore band
Ri
compact layer
CPEi
Rct
CPEdl
Mg substrate

Fig. 11

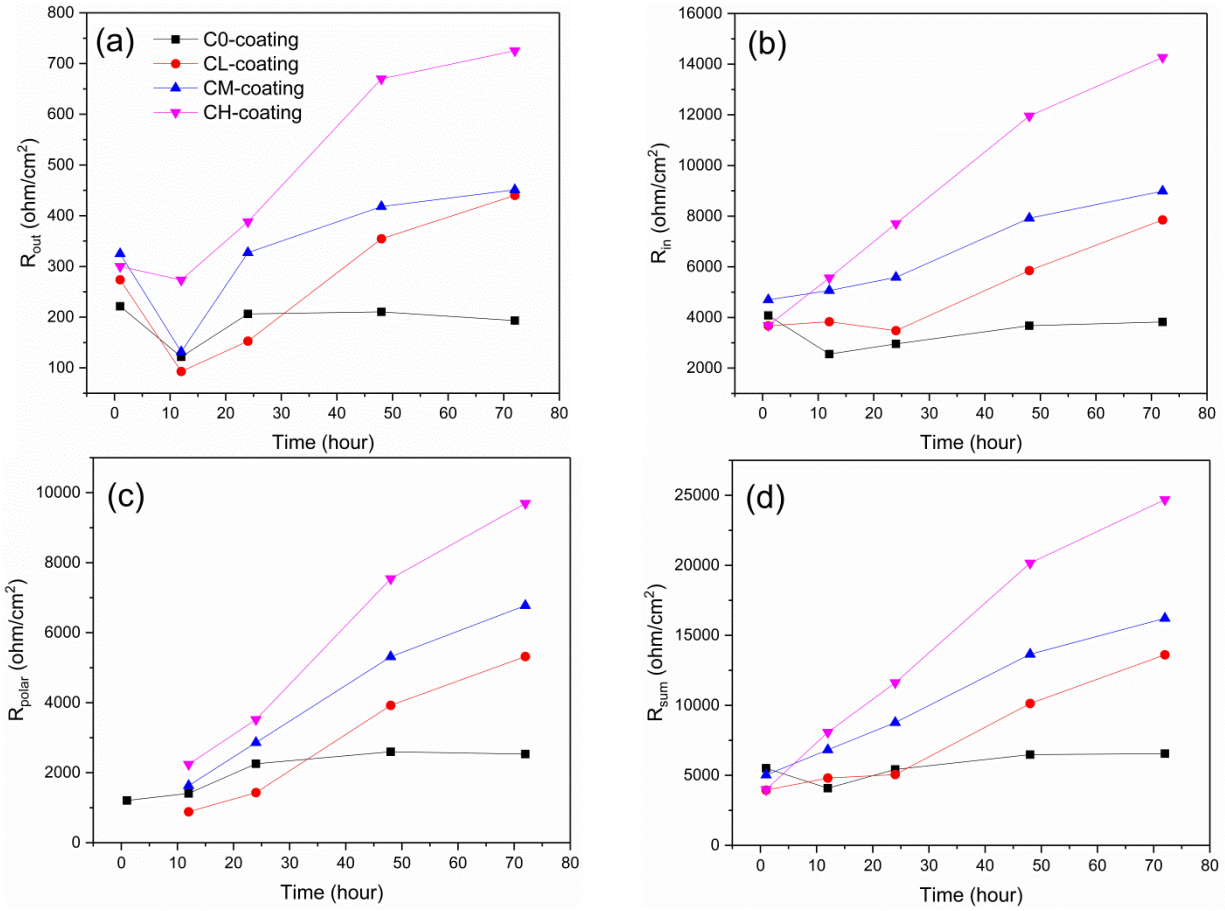
(a)
C0-coating
CL-coating
CM-coating
CH-coating
R_{out} (ohm/cm^2)
Time (hour)
(b)
R_{in} (ohm/cm^2)
Time (hour)
(c)
R_{polar} (ohm/cm^2)
Time (hour)
(d)
R_{sum} (ohm/cm^2)
Time (hour)

Fig. 12

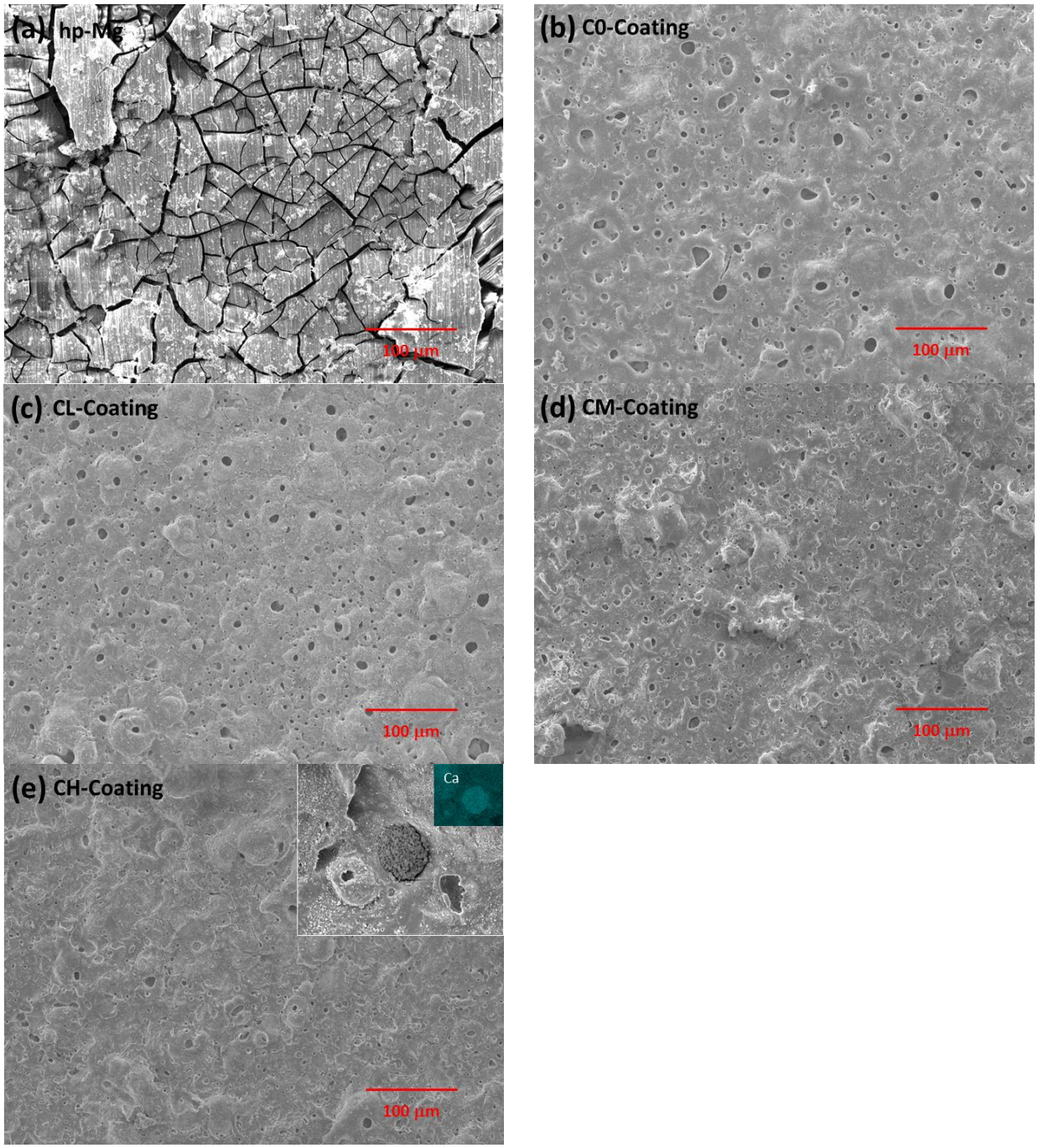
(a) hp-Mg
100 µm
(b) C0-Coating
100 µm
(c) CL-Coating
100 µm
(d) CM-Coating
100 µm
(e) CH-Coating
Ca
100 µm
Fig. 13

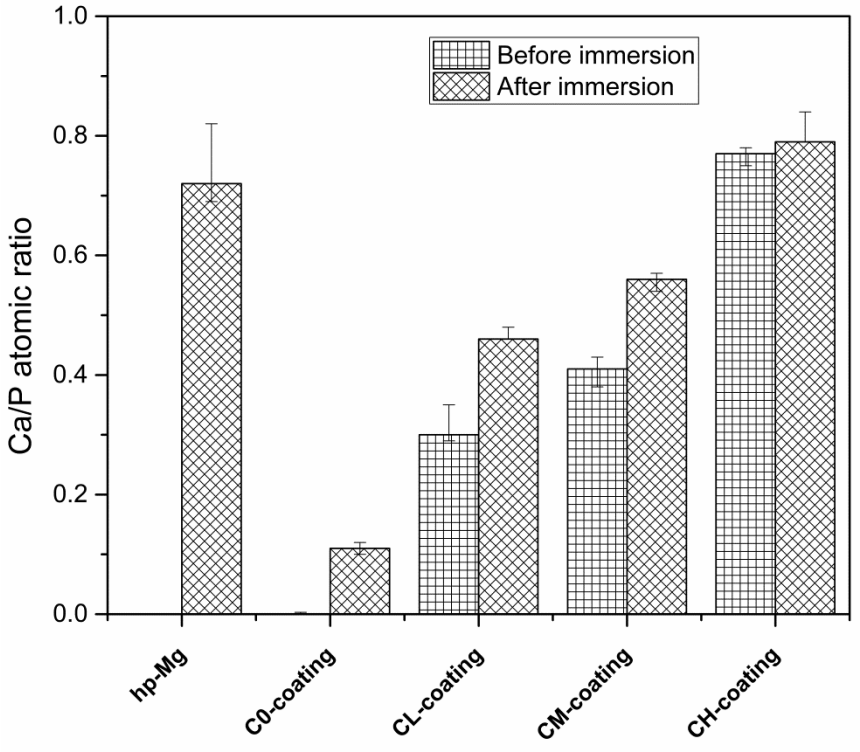
Before immersion
After immersion
Ca/P atomic ratio
1.0
0.8
0.6
0.4
0.2
0.0
hp-Mg
C0-coating
CL-coating
CM-coating
CH-coating

Fig. 14

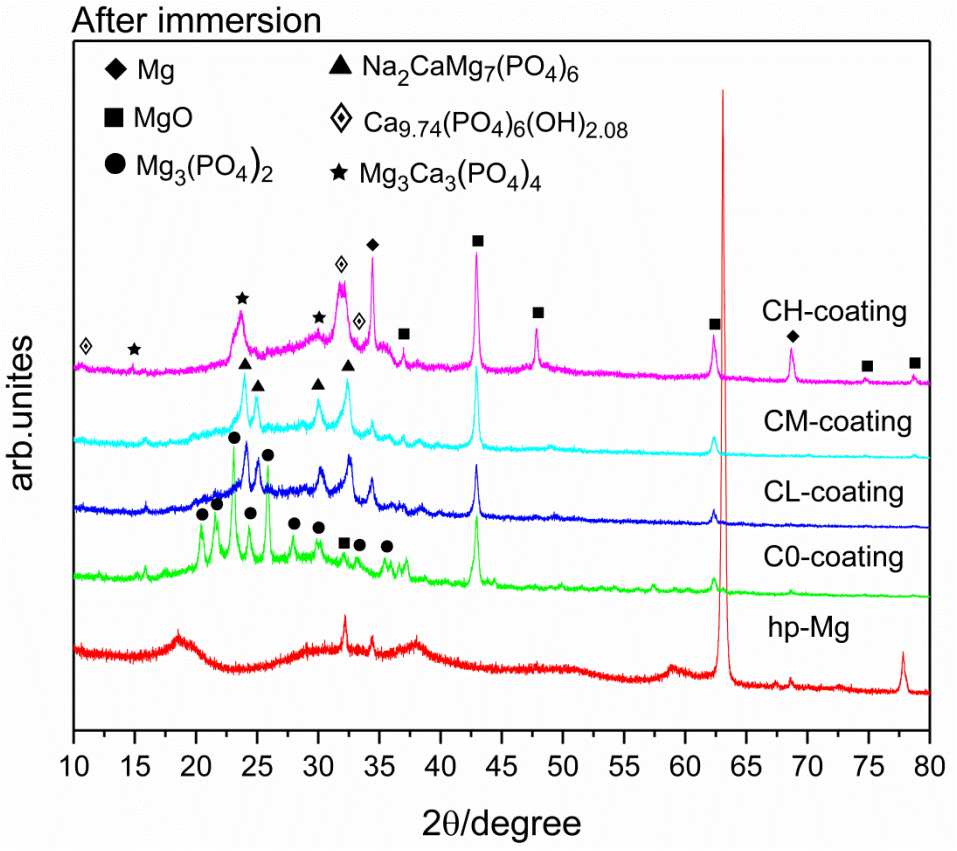
After immersion
Mg
MgO
Mg3(PO4)2
Na2CaMg7(PO4)6
Ca9.74(PO4)6(OH)2.08
Mg3Ca3(PO4)4
CH-coating
CM-coating
CL-coating
C0-coating
hp-Mg
arb.unites
10 15 20 25 30 35 40 45 50 55 60 65 70 75 80
2θ/degree

Fig. 15

Table 1 Electrolyte composition and power parameters for PEO processing

Sample	Electrolyte (g/L)			pH	Conductivity (ms/cm)	Power mode and parameters
	KOH	Na_3PO_4	HAp			
C0-coating	2	10	-	12.30	19.06	0.75A (constant current)
CL-coating	2	10	5	12.30	18.58	
CM-coating	2	10	10	12.33	18.10	
CH-coating	2	10	20	12.47	18,02	

Table 2 Elemental composition (at.%) of PEO-(HAp) examined by EDS

	O	Na	Mg	P	K	Ca
C0-Coating	49.962	5.371	29.534	14.229	0.904	-
CL-Coating	50.915	5.086	23.708	15.411	0.252	4.628
CM-Coating	51.314	4.402	20.566	15.818	0.157	7.743
CH-Coating	51.356	2.912	20.282	14.414	-	11.036